HHS Public Access

Author manuscript

Nat Commun. Author manuscript; available in PMC 2014 January 27.

Published in final edited form as:

Nat Commun. 2013 ; 4: 2231. doi:10.1038/ncomms3231.

The RAG2 C-terminus and ATM protect genome integrity by controlling antigen receptor gene cleavage

Julie Chaumeil[1], **Mariann Micsinai**[1,2,3,5], **Panagiotis Ntziachristos**[1], **David B. Roth**[6], **Iannis Aifantis**[1,4], **Yuval Kluger**[5], **Ludovic Deriano**[7], and **Jane A. Skok**[1,3,†]

[1]Department of Pathology, New York University School of Medicine, New York, NY 10016, USA

[2]Center for Health Informatics and Bioinformatics, New York University School of Medicine, New York, NY 10016, USA

[3]NYU Cancer Institute, New York University School of Medicine, New York, NY 10016, USA

[4]Howard Hughes Medical Institute, New York University School of Medicine, New York, NY 10016, USA

[5]Department of Pathology and Yale Cancer Center, Yale University School of Medicine, New Haven, CT 06520, USA

[6]Department of Pathology and Laboratory Medicine and Abramson Family Cancer Research Institute, Raymond and Ruth Perelman School of Medicine, University of Pennsylvania, Philadelphia, PA 19104, USA

[7]Department of Immunology and Department of Genomes & Genetics, Institut Pasteur, CNRS-URA1961, Paris 75015, France

Abstract

Tight control of antigen-receptor gene rearrangement is required to preserve genome integrity and prevent the occurrence of leukemia and lymphoma. Nonetheless, mistakes can happen, leading to the generation of aberrant rearrangements, such as *Tcra/d-Igh* inter-locus translocations that are a hallmark of ATM deficiency. Current evidence indicates that these translocations arise from the persistence of unrepaired breaks converging at different stages of thymocyte differentiation. Here we show that a defect in feedback control of RAG2 activity gives rise to bi-locus breaks and damage on *Tcra/d* and *Igh* in the same T cell at the same developmental stage, which provides a direct mechanism for generating these inter-locus rearrangements. Both the RAG2 C-terminus and ATM prevent bi-locus RAG-mediated cleavage through modulation of 3D conformation (higher order loops) and nuclear organization of the two loci. This limits the number of potential substrates for translocation and provides an important mechanism for protecting genome stability.

†To whom correspondence should be addressed: Tel: 212-263-0504, jane.skok@med.nyu.edu.

Author Contribution: JC and JS conceived the study and wrote the manuscript. JC performed most of the experiments. MM analyzed the 4C-seq and ChIP-seq data. PN performed the ChIP-seq experiments. LD analyzed the damage experiments, performed the ATM western blot, provided *Atm*$^{-/-}$, *Rag2*$^{c/c}$ and *Rag2*$^{c/c}$ *p53*$^{-/-}$ mice and revised the manuscript. DBR, IA and YK provided technical and conceptual support. All the authors read and approved the manuscript.

Competing Interests Statement: The authors declare that they have no competing financial interests.

B and T lymphocyte development is driven by V(D)J recombination, a process through which V, D and J coding segments within each of the seven antigen receptor loci, are rearranged to create a vast repertoire of antigen receptors[1,2]. Generation of receptor diversity through recombination is critical for shaping the adaptive arm of the immune system, enabling B and T cells to mount a focused and specific response to foreign antigen. This programmed rearrangement event relies on the lymphoid-specific proteins, RAG1 and RAG2 (Recombination Activating Genes 1 and 2), which individually harbor many distinct regulatory domains whose functions remain largely enigmatic. Nonetheless, it is known that at least some of these contribute to the performance of RAG through fine-tuning of targeting, cleavage and repair. Furthermore, the proper functioning of the recombinase complex relies on cooperation between the two proteins, RAG1 and 2.

Specificity of targeting is conferred by RAG1 mediated recognition of highly conserved recombination signal sequence (RSS) elements that flank the individual V, D and J gene coding segments, which are arrayed along each antigen receptor locus[3-5]. Moreover, RAG1 carries the catalytic endonuclease activity[4,5]. However, cleavage cannot occur in the absence of its partner protein, RAG2[6,7], which contains a PHD domain (Plant Homeo Domain) that is known to direct binding of the recombinase to active chromatin through recognition of the histone modification, H3K4me3[8,9]. The RAG1/2 complex binds to two gene segments (that can be many kilobases apart) brings them together and cuts at the RSS borders to generate DNA double-strand breaks (DSBs). Following cleavage the four resulting broken ends are held together in a RAG post-cleavage complex which is instrumental in directing repair by the ubiquitous non-homologous end joining (NHEJ) pathway[1,2,10,11]. The introduction of DSBs activates several PI3K-like Ser/Thr kinases, including the ATM kinase (Ataxia telangiectasia mutated), which phosphorylate downstream proteins and orchestrate the DNA damage response[2]. Other DNA damage response factors, like the histone variant γ-H2AX, 53BP1 (p53 binding protein 1), and the MRN complex (containing Mre11, Rad50 and Nbs1), are rapidly recruited and form nuclear foci at the site of DSBs[2,11].

Recombination is tightly regulated so that the appropriate loci and gene segments are rearranged in the appropriate lineage (*T cell receptor* (*Tcr*) loci in T cells and *immunoglobulin* (*Ig*) loci in B cells) and at the appropriate developmental stage. In T cells productive rearrangement of the different *Tcr* loci gives rise to two distinct lineages: recombination of *Tcrg*/*Tcrd* and *Tcrb/Tcra* leads to γδ and αβ T cells, respectively[12,13]. Despite this separation, recombination of the different loci overlaps. *Tcrg*, *Tcrd* and *Tcrb* are all rearranged at the early $CD4^{-}CD8^{-}$ double negative DN2/3 stage of development, while *Tcra* recombination occurs later in double positive (DP) cells[14].

Regulation of *Tcrd* and *Tcra* recombination is uniquely complicated because, beyond the fact that they recombine at different stages of differentiation, *Tcra* and *Tcrd* share the same chromosomal location, with the latter embedded between the Vα and Jα gene segments. Furthermore, promiscuous D_H-to J_H rearrangement of the *Igh* locus, which occurs at low level in T lineage cells[15], adds yet another layer of complexity. Together these issues compound the risks associated with *Tcra/d* recombination and the probability of aberrant repair. Indeed, inter-locus rearrangements between *Tcra/d* and *Igh* have been identified as a

hallmark of thymic lymphomas in ATM-deficient mice[16]. Moreover, we recently discovered translocations between these two loci associated with an absence of the non-core C-terminal domain of RAG2[17]. Although this domain is dispensable for recombination[18,19], its deletion is known to affect the joining step, as well as the order, efficiency and fidelity of the reaction[10,20-25]. When coupled with the disruption of p53, we found that *Rag2*$^{c/c}$ *p53*$^{-/-}$ mice develop thymic lymphomas harboring recurrent translocations involving *Tcra/d* and *Igh*, defects that are similar to those found in *Atm*$^{-/-}$ mice[17]. In addition, ATM and the C-terminus of RAG2 have similar defects in stabilizing the RAG post-cleavage complex[17,26].

Here we have now investigated the mechanisms underlying the origins of the inter-locus *Igh-Tcra/d* translocations prior to lymphomagenesis to determine whether regulation of cleavage and nuclear accessibility of the loci is perturbed by an absence of ATM and the C-terminus of RAG2. We find that *Igh* cleavage occurs at higher levels in DN2/3 versus DP cells and thus its rearrangement could overlap with *Tcra/d* rearrangement. However breaks are not found in *Igh* and *Tcra/d* in the same cell, except in the absence of the RAG2 C-terminus or ATM. Control of mono-locus cleavage involves regulated mono-locus looping out from the chromosome territory and mono-locus association with repressive pericentromeric heterochromatin. In the absence of the RAG2 C-terminus or ATM nuclear accessibility is increased and both loci remain euchromatic and bi-locus loops can be detected coincident with bi-locus cleavage. Interestingly we found that expression of RAG brings *Tcra/d* and *Igh* into close proximity in DN2/3 cells (when RAG-mediated cleavage *Igh* occurs at high levels) while the two loci separate at the subsequent DP cell stage of development (when recombination of *Igh* is reduced). In contrast, in the mutant cells increased association of *Tcra/d-Igh* in DP cells is linked to increased nuclear accessibility, and the introduction of bi-locus breaks and damage on proximal loci. In sum, this study show a role for the non-core domain of RAG2 and of ATM in controlling recombination between two loci via modulation of nuclear organization. Moreover, these events provide a direct mechanism for the generation of the *Tcra/d-Igh* translocations that are found in *Rag2*$^{c/c}$ *p53*$^{-/-}$ and *Atm*$^{-/-}$ tumors.

Results

Igh and *Tcra/d* rearrangement overlaps in DN2/3 and DP cells

Although it is established that the *Igh* locus (which is located on chromosome 12) undergoes low level D_H-J_H rearrangement (at the 3′ end of the locus) in T cells, it is not known at which stage of development recombination occurs. To determine this, we performed an immuno-DNA FISH experiment to analyze RAG mediated cleavage on *Igh* in wild-type DN2/3 and DP cells (Fig. 1a) using a DNA probe that hybridizes to the 3′ end of this locus (See scheme Fig. 1b) in combination with an antibody against the phosphorylated form of H2AX, γ-H2AX, as a read-out for double-stranded breaks (DSBs)[27,28]. Our analyses showed that RAG-mediated γ-H2AX foci were associated more frequently with *Igh* in DN2/3 compared to DP cells suggesting that D_H-J_H rearrangement occurs predominantly, but not exclusively, at the earlier stage of development (Fig. 1c and Supplementary Table S1). In contrast, RAG-mediated γ-H2AX foci were associated more frequently with *Tcra/d* in DP compared to DN2/3 cells (Fig. 1b,c and Supplementary Table S1).

The RAG2 C-terminus and ATM regulate mono-locus cleavage

As *Tcra/d* and *Igh* loci both undergo recombination in T cells, it is conceivable that there is overlap in the timing of their rearrangement. If so, bi-locus breaks could be introduced concurrently in the same cell and in the event of a defect in joining, these could act as substrates for translocations. However, when we examined the frequency of γ-H2AX foci associated with both *Tcra/d* and *Igh* (bi-locus breaks) in individual wild-type DN2/3 and DP cells we found these present at a very low level which was only slightly above the frequency of bi-locus breaks detected in RAG-deficient cells (Fig. 2a and Supplementary Tables S2, S3). In contrast, we found a significant rise in the frequency of bi-locus breaks in individual *Rag2*$^{c/c}$ *p53*$^{-/-}$ or *Atm*$^{-/-}$ cells, with the most pronounced increase occurring at the DP stage, at the time of *Tcra* recombination (Fig. 2a,b and Supplementary Tables S2, S3). It is of note that we found no increase in the frequency of bi-locus breaks in the absence of another DNA damage response factor, 53BP1, which is known to be important for the long-range joining of coding ends in V(D)J recombination[29] (Fig. 2a and Supplementary Tables S2, S3). These data indicate that bi-locus breaks in the same cell do not occur simply as a result of a defect in repair.

Since cells deficient in both p53 and ATM have defects in cell cycle checkpoints that enable unrepaired breaks to be propagated as a result of cell division[30,31] it is possible that some proportion of the bi-locus breaks that we detected in mutant DP cells could be attributed to the persistence of unrepaired breaks being amplified in proliferating DN4 cells, which mark the transition from the DN2/3 to the DP stage of development (Fig. 1a). To check this we compared the frequency of bi-locus breaks in individual *Rag2*$^{c/c}$ versus *Rag2*$^{c/c}$ *p53*$^{-/-}$ cells. However, we found no significant differences in the incidence of bi-locus breaks in the two genotypes so we conclude that the increase in bi-locus breaks that we detected in *Rag2*$^{c/c}$ *p53*$^{-/-}$ DP cells does not result from an absence of p53 (Fig. 2a and Supplementary Tables S2, S3). Indeed, we also found no significant increase in bi-locus breaks on *Tcra/d* and *Igh* in wild-type versus *p53*$^{-/-}$ cells (4% compared to 4.6%, respectively). In addition, differences in the level of ATM in *Rag2*$^{c/c}$ versus wild-type cells cannot explain the differences in the frequency of bi-locus breaks as Western blot analysis showed similar levels of protein in the two genotypes (Supplementary Fig. S1). Taken together these data indicate that the C-terminus of RAG2 and ATM regulate cleavage to ensure that RAG mediated breaks are introduced on only one locus at a time in each recombining T cell.

The RAG2 C-terminus and ATM regulate *Tcra-Igh* association

We and others have shown that nuclear proximity of broken partner genes is an important factor in translocations[32-37]. Since our studies indicate that translocations between *Tcra/d* and *Igh* are found in tumors from *Rag2*$^{c/c}$ *p53*$^{-/-}$ and *Atm*$^{-/-}$ mice[17] we wanted to examine the association between the two loci in recombining DN2/3 and DP cells. For this we performed circularized chromosome conformation capture with next generation sequencing (4C-seq), using a bait sequence spanning the *Tcra* enhancer (Eα) at the 3′α end of the locus (see Methods section for details; Fig. 3a, Supplementary Fig. S2a and Supplementary Table S4). The 4C data is displayed as a domainogram, which is a statistical way to visualize local 4C signal enrichment across a region of interest[38]. It is clear from Fig. 3a (left panels) that there are significant changes in the interaction partners of *Tcra/d* in the two populations

across chromosome 12. Importantly, the intensity of the *Tcra*/*d*-*Igh* interaction is much higher in DN2/3 cells where, according to our γ-H2AX analysis, the latter is recombined at higher frequency (Fig. 3a (right panels)). This result was validated by additional 3-D DNA FISH experiments, and distances separating the two loci were plotted as cumulative frequency curves, using a cut-off of 1μ m to measure close association (ie. 'pairing') (Supplementary Fig. S2b). On these graphs a left shift is indicative of closer association. Examples of paired and unpaired loci are shown in Fig. 3b.

Previous studies indicate that RAG binds to active chromatin and localizes to the J segments at the 3′ end of each antigen receptor locus in rearranging cells[39]. We have recently shown that localized RAG enrichment in this region is linked with homologous *Tcra* pairing, transcription and regulated mono-allelic cleavage in DP cells[40]. Thus, we wanted to investigate whether the presence of RAG could influence the frequency with which *Tcra/d* and *Igh* contact each other during recombination. There are two regions of RAG2 binding on the *Igh* locus in developing T cells (Fig. 3c). The first corresponds to enrichment of H3K4me3 and H3K9ac at the 3′ end of *Igh*, where D_H-J_H rearrangement is known to occur in these cells[15]. In addition, RAG2 also binds to the V_H portion of *Igh* and this could explain the high frequency of interaction with *Tcra* in this region (Fig 3a and Supplementary Table S5). Interestingly, we found that an absence of RAG1 significantly decreased heterologous association of the two loci in DN2/3 cells while we observed no significant change in DP cells (Fig. 3d and Supplementary Fig. S2c). These data indicate that RAG1 brings recombining *Tcra/d* and *Igh* together in DN2/3 cells (where *Igh* cleavage occurs at high levels) but that these loci separate in DP cells (where cleavage of *Igh* is reduced and cleavage of *Tcra* occurs at high levels) (Fig. 1c). Intriguingly, the absence of the C-terminus of RAG2 or ATM deficiency did not affect the frequency of *Tcra*/*d*-*Igh* association in DN2/3 cells, however in DP cells, where association of the two loci is normally reduced, we observed an increase in the incidence of heterologous pairing in both mutants, while pairing in the equivalent 53BP1-deficient populations followed the same pattern as in wild-type cells (Fig. 3e). Importantly, bi-locus breaks were increased on heterologously paired loci in *Rag2*$^{c/c}$ *p53*$^{-/-}$ and *Atm*$^{-/-}$ DP cells compared with wild-type control and 53BP1-deficient cells (Fig. 4a,b and Supplementary Table S6). In sum, these data indicate that an increased frequency in contact between *Tcra* and *Igh* in *Rag2*$^{c/c}$ *p53*$^{-/-}$ and *Atm*$^{-/-}$ DP cells is linked to an increased frequency in bi-locus breaks on paired loci.

RAG-mediated pairing is not a general phenomenon

Genome wide analysis has shown that RAG2 has an overlapping pattern with H3K4me3 enriched regions[39], thus we wanted to determine whether other RAG enriched active genes would pair up with *Tcra* in the same way as *Igh*. For this analysis we selected five hematopoietic lineage specific genes (*Hmgb1*, *Lat*, *Cd3g*, *Ly6d* and *Satb1*) as well as a housekeeping gene (*Gapdh*) that are all located on different chromosomes and transcribed in these cells (Fig.5a,b). Interestingly, pairing of *Tcra* with these other RAG-enriched loci shows an opposite trend to *Igh*-*Tcra* pairing in all cases (Fig. 5c and Supplementary Table S7). Indeed, in contrast to *Tcra*-*Igh* an absence of RAG1 appears to increase their contact frequency with *Tcra* in DN2/3 cells and association is even more pronounced at the DP stage of development. Furthermore, pairing between these control loci follows the same

trend as their association with *Tcra* (Fig. 5d and Supplementary Table S7). It is of note that the maximum frequency of pairing (for individual pairs of alleles) in all cases is very similar (around 20%) and this matches the maximum level of homologous *Tcra* pairing seen during recombination in DP cells[40]. Taken together these data indicate that the trend for *Tcra-Igh* is unique and even though RAG2 is enriched on control loci, pairing does not depend on the presence of RAG. Instead, interactions between control loci may be influenced by binding of other transcription factors that are involved in their regulation. In this context the Fraser lab have shown that co-ordinately regulated genes associate with each other in common transcription factories and more recent studies from the Murre lab indicate that transcription factor bound regions determine intra- and inter-domain interactions that are developmentally regulated[4142]. Thus, perhaps other transcription factors that are enriched on these control genes may be dominant in determining their interaction partners in developing T cell nuclei.

Regulation of RAG cleavage is linked to genome stability

The *Tcra* and *Igh* loci are located on different chromosomes, namely chromosomes 14 and 12 respectively. To understand how association between these two loci occurs in nuclear space we focused our attention on the formation of higher order loops which moves genes outside of their chromosome territories as a mechanism by which they could be brought into close contact. We recently showed that mono-locus looping out of *Tca* is linked to homologous pairing during recombination[40]. To examine this we measured the distance separating the 3′ end of *Tcra* and *Igh* from their respective chromosome 14 and 12 territories when the loci were paired. Our analyses indicate that in wild-type DP cells the vast majority of higher-order loop formation occurred on one locus at a time and these predominantly involved *Tcra* (Fig. 6a,b and Supplementary Table S8), the locus in which we detected the most breaks (Fig. 4a). In contrast, there was a significant increase in bi-locus loop formation on paired *Tcra-Igh* alleles in *Rag2*$^{c/c}$ *p53*$^{-/-}$ and *Atm*$^{-/-}$ DP cells (Fig. 6a,b and Supplementary Table S8) coincident with an increase in bi-locus breaks (Fig. 4a). Taken together our data indicate that an increase in *Tcra-Igh* pairing in *Rag2*$^{c/c}$ *p53*$^{-/-}$ and *Atm*$^{-/-}$ DP cells is linked to an increase in bi-locus looping and bi-locus breaks on paired alleles.

Higher-order looping of genes away from their chromosome territories has previously been correlated with open chromatin and an active transcriptional status, while silent genes are positioned more internally[43-46]. To determine whether nuclear accessibility of the individual loci is linked to loop formation we examined the location of paired *Tcra-Igh* relative to repressive pericentromeric heterochromatin (PCH). In wild-type DP cells we found that paired *Tcra-Igh* alleles were frequently located at PCH, however the two loci were not equivalently close (Fig. 6c,d and Supplementary Table S9). Interestingly, we found that the *Igh* locus was predominantly in contact with PCH while *Tcra*, the locus associated with the most loops and breaks in these pairs, remained euchromatic. In contrast, in *Rag2*$^{c/c}$ *p53*$^{-/-}$ and *Atm*$^{-/-}$ DP cells, repositioning of the *Igh* to PCH was significantly reduced and this increased nuclear accessibility was associated with increased bi-locus breaks (Fig. 6c,d). In sum, these data indicate that the increase in bi-locus breaks on paired *Tcra-Igh* alleles in *Rag2*$^{c/c}$ *p53*$^{-/-}$ and *Atm*$^{-/-}$ DP cells is linked with an increase in the simultaneous nuclear accessibility of the two loci, as assessed by looping out from their chromosome territories and by their location away from repressive PCH.

Since close proximity of broken partner loci in DP cells could provide a fertile ground for the generation of the aberrant inter-locus rearrangements that are a characteristic of *Rag2*$^{c/c}$ *p53*$^{-/-}$ and *Atm*$^{-/-}$ lymphomas we next asked whether the increase in bi-locus breaks and increased accessibility of paired *Tcra/d*/*Igh* was linked with an increase in bi-locus instability in interphase *Rag2*$^{c/c}$ *p53*$^{-/-}$ and *Atm*$^{-/-}$ cells prior to the onset of lymphomagenesis. For this, we performed a DNA FISH experiment using BAC probes that hybridize outside the 3′ and 5′ ends of each locus (See scheme Fig. 1b) and examined the frequency of damage (ie. split alleles (> 1.5μm in between the two ends), duplicated or missing signals). The increase in bi-locus damage in individual *Rag2*$^{c/c}$ *p53*$^{-/-}$ and *Atm*$^{-/-}$ mutant DP cells was very significant (Fig. 6e,f and Supplementary Table S10). Thus an absence of the C-terminal domain of RAG2 or ATM results in an increase in both bi-locus breaks and bi-locus damage in the same cell.

Discussion

Taken together our data show that translocations between *Tcra/d* and *Igh* that are found in tumors from *Rag2*$^{c/c}$ *p53*$^{-/-}$ and *Atm*$^{-/-}$ mice[17] may arise not only as a result of *Tcrd* recombination (as shown previously in ATM-deficient mice[16]) but also from *Tcra* recombination. It has previously been proposed that the aberrant interlocus *Tcra/d-Igh* rearrangements found in *Atm*$^{-/-}$ T cells arise from the persistence of unrepaired breaks converging at different stages of thymocyte differentiation[16]. However, in contrast to our analyses, these studies did not examine breaks on *Tcra/d* and *Igh* in individual developing T cells, but rather they analyzed translocations in *Atm*$^{-/-}$ mature T cells and *Atm*$^{-/-}$ derived thymic lymphomas, respectively. Here we show that breaks on the two loci occur in the same cell at the same stage of development, which provides a direct mechanism for the generation of the characteristic inter-locus *Tcra/d-Igh* translocations that are found in *Rag2*$^{c/c}$ *p53*$^{-/-}$ and *Atm*$^{-/-}$[17,47,48] T-lymphomas.

Our studies reveal that there is similarity between the C-terminus of RAG2 and ATM in temporally harnessing RAG activity to ensure that cleavage occurs on only one locus at a time in recombining T cells. Intriguingly we find that RAG mediated association of recombining loci in localized ‘recombination centers’ is linked to feedback control of RAG cleavage: the introduction of a break on one locus is coupled with repositioning of the partner locus to PCH and inhibition of bi-locus cleavage and looping out from the territory (see Model in Supplementary Fig. S3). Targeting of RAG to the correct allele (*Tcra* rather than *Igh*) is likely to be influenced by the higher level of transcription on *Tcra*. Interestingly, although cleavage of *Tcra* is reduced in paired *Tcra/d-Igh* alleles in *Rag2*$^{c/c}$ *p53*$^{-/-}$ DP cells (perhaps due to a decrease in efficiency of cleavage in the absence of the C-terminus of RAG2), there is a significant increase in cleavage of *Igh*, which further underlines the role of regulation *in trans* between the two loci. Although we recently showed that pairing and higher-order looping of *Tcra* homologous alleles is linked with regulation of their recombination[40], cross-talk and regulation of heterologous loci *in trans* has not previously been shown to be linked to the formation of higher-order looping. Indeed higher-order loop formation was previously shown to be involved in stochastic interactions between different loci on separate chromosomes[41,49] while here we have found that interactions between *Tcra/d* and *Igh* are mediated by the presence of RAG.

Together our data suggest that regulation of mono-locus cleavage relies on changes in nuclear organization that are associated with a reduction in accessibility. Regulation of mono-locus cleavage is thus akin to regulation of mono-allelic cleavage. Indeed, our previous studies showed that ATM recruited to the site of a break on one allele acts *in trans* to reposition the second homologous allele to PCH and to prevent the introduction of further breaks on the partner homologue[40,50]. We propose that homologous and heterologous antigen receptor alleles come together in localized recombination centers for coordinated regulation of RAG cleavage. Here we have now identified an auto-regulatory role for RAG2 in restricting cleavage in an analogous manner to ATM. These data explain the mechanisms underlying the origins of the inter-locus *Igh-Tcra/d* in *Atm*$^{-/-}$ and *Rag2*$^{c/c}$ *p53*$^{-/-}$ lymphocytes prior to lymphomagenesis. Importantly, they identify an unappreciated role for the C terminal of RAG2 in regulating chromosome dynamics and accessibility of target loci to restrict ongoing cleavage after the introduction of a break on one locus. Thus feedback control of RAG activity relies on signals transmitted via the RAG complex itself.

Regulation of V(D)J recombination occurs at multiple levels to prevent the occurrence of chromosomal translocations or deletions that can result from errors in repair and/or mis-targeting of RAG1/2 to cryptic RSSs. However, beyond degradation of RAG2 protein[8] and our more recent findings that expression of *Rag1* is regulated across cell cycle[51], there been have no studies that focus specifically on auto-regulation of RAG cleavage activity in individual cells. It is clearly critical to have such mechanisms in place to ensure that further breaks are not introduced in *cis*, or in *trans* on accessible target loci that undergo recombination at overlapping stages of development (*Tcrg, Tcrb, Tcrd* and *Igh* in DN T cells and *Igk* and *Igl* in pre-B/immature B cells). Furthermore, this same mechanism could also be important in preventing cleavage on actively transcribed off-target loci with cryptic RSSs that bind RAG.

Methods

Mice

The *Atm*$^{-/-}$, *Rag2*$^{c/c}$ and *Rag2*$^{c/c}$ *p53*$^{-/-}$ mice were provided by Ludovic Deriano and David Roth[17]. RAG1-deficient mice were provided by Yanhong Ji, Grace Teng and David Schatz: RAG1-deficient DP cells (R1$^{-/-}$ β and control WT β) were derived from mice carrying a functionally rearranged *Tcrb* transgene (β) that allows T cell development to proceed to the DP stage in the absence of *Tcrb* rearrangement. The *53BP1*$^{-/-}$ mice were provided by Davide Robbiani and Michel Nussenzweig[52]. Wild-type littermates were used as controls. Animal care was approved by NYU School of Medicine Animal Care and Use Committee of (protocol number 120315-01).

T cell flow cytometry sorting

Flow cytometry cell sorting was performed on a MoFlo or Reflection sorter. Antibodies were as follows: Thy1.2 PE-Cy7 (CD90.2, clone 53-2.1, eBioscience, 1:1000 dilution), TCRβ APC-eFluor780 (clone H57-597, eBioscience, 1:500 dilution), CD4 APC (L3T4, RM4-5, BD Biosciences, 1:500 dilution), CD8a FITC (clone 53-6.7, BD Biosciences, 1:500 dilution), CD25 PE (PC61, BD Biosciences, 1:500 dilution). The gating strategy was:

Thy1.2^{+}/TCRβ^{int}/CD4^{+}/CD8^{+} for DP cells and Thy1.2^{+}/TCRβ^{low}/CD4^{-}/CD8^{-}/CD25^{+} for DN2/3 cells.

3-D DNA FISH and immuno-FISH

3D-DNA FISH and combined DNA FISH-immunofluorescence for γ-H2AX (immuno-FISH) were carried out on T cells adhered to poly-L lysine coated coverslips, as previously described[50,53]. Briefly, cells were fixed with 2% paraformaldehyde / PBS (pH 7-7.4) for 10 minutes at room temperature (RT) and permeabilized for 5 minutes with 0.4% Triton / PBS on ice. After 30 minutes of blocking in 2.5% BSA / 10% normal goat serum / 0.1% Tween-20 / PBS, cells were sequentially incubated with a primary antibody against phosphorylated serine-139 of H2AX (γ-H2AX; Millipore) and a secondary goat-anti-mouse antibody (Alexa Fluor 488 or 555; Invitrogen) for one hour at RT each. Cells were then post-fixed in 2% paraformaldehyde / PBS for 10 minutes at RT, incubated with 0.1 mg/ml RNaseA for 30 minutes at 37°C and permeabilized in 0.7% Triton-X-100 / 0.1M HCl for 10 minutes on ice. Cells were then denatured with 50% formamide / 2×SSC (pH 7-7.4) for 30 minutes at 80°C, and hybridized overnight with the probes at 37°C. The next day, cells were rinsed 3 times in 50% formamide / 2×SSC and 3 times in 2×SSC at 37°C for 5 minutes each. Finally slides were mounted in ProLong Gold (Invitrogen) containing 1.5 μg/ml DAPI.

Probes

BAC probes RP23-255N13 (3′α *Tcra*), RP23-304L21 (5′α *Tcra*), CT7-34H6 (3′ *Igh*), RP24-386J17 (5′ *Igh*), RP24-289O10 (*Hmgb1*), RP24-358H24 (*Gapdh*), RP24-342A2 (*Lat*), RP23-410N16 (*Cd3g*), RP24-277H9 (*Ly6d*), and RP23-137H17 (*Satb1*) were directly labeled by nick translation with ChromaTide Alexa Fluor 488 or 594-5-UTP (Molecular Probes) or Cy3- or Cy5-dUTP (Fisher). For one coverslip, 0.5 μg of nick-translation product was precipitated and resuspended in 10 μl of hybridization buffer (50% formamide / 20% dextran sulfate / 5× Denharts solution), denatured for 5 minutes at 95°C and pre-annealed for 45 minutes at 37°C before overnight hybridization with cells. XCyting Mouse Chromosomes 14 (Texas-red) and 12 (FITC) paints (Metasystems) were prepared separately following supplier's instructions. Paint and BAC probes were combined just prior to overnight hybridization.

Confocal microscopy and analysis

3-D images were acquired by confocal microscopy on a Leica SP5 AOBS system (Acousto-Optical Beam Splitter). Optical sections separated by 0.3 μm were collected and stacks were analyzed using Image J software. Alleles were defined as associated with γ-H2AX if the BAC signals and immunofluorescence foci were at least partially overlapped (at least one pixel of colocalization). Alleles were considered as located at pericentromeric heterochromatin (PCH) when BAC signals were adjacent or overlapping with a γ-satellite signal (no pixel in between the edges of the BAC and γ-satellite signals). Distances from the loci to their chromosome territories (higher-order looping) were measured from the centre of mass of the BAC signal to the closest edge of the chromosome paint. Distances between alleles or loci were measured between the center of mass of each BAC signal.

Statistical analyses

The statistical tests were applied to combined data sets from repeated experiments. Supplementary tables display individual experiments to show the low level of variation between the repeats. Statistical analyses were performed using a two-tail Fisher-exact test: *P*-values ≤ 5.00e-2 (a = 0.05) were taken to be significant (1.00e-2 ≤ *P* ≤ 5.00e-2 * significant; 1.00e-3 ≤ *P* ≤ 1.00e-2 ** very significant; *P* < 1.00e-3 *** highly significant).

Circularized chromosome conformation capture (4C-seq)

4C-seq and domainogram analyses were performed as previously described[35,40,54]. **Fixation and cell lysis** - 10^7 cells were resuspended in 5ml PBS-10% FBS and fixed in 5ml 4% formaldehyde-10%FBS for 10min at RT (tumbling). 1.425ml 1M glycine was added to quench cross-linking and tubes were put on ice for 2min. After 8min centrifugation at 1300RPM at 4°C, pellets were resuspended in 1ml cold “lysis buffer” (50mM Tris pH7.5, 150mM NaCl, 5mM EDTA, 0.5% NP-40, 1% Triton X-100, 1 tablet mini complete) and incubated for 20min on ice. After 5min centrifugation at 1800RPM at 4°C, pellets were resuspended in 360µl sterile water (or stored at −80°C). **HindIII digestion** - Nuclei were incubated for 1h at 37°C with 60µl 10× restriction buffer B and 15 µl 10% SDS (shaking). 150 µl 10% Triton X-100 were added and nuclei were incubated for 1h at 37°C (shaking). 5 µl of the sample were taken as the “undigested control”. Nuclei were incubated overnight at 37°C with 400U of HindIII restriction enzyme. Fresh enzyme was added for 6 more hours during the day. 5 µl “undigested” and “digested” controls were incubated in 90 µl Tris pH7.5 and 5 µl 10mg/ml Proteinase K for 2h at 65°C, DNA was extracted with 100 µl phenol-chloroform and the water phase was loaded on a 0.6% agarose gel. The HindIII enzyme was inactivated by adding 80 µl 10% SDS and incubating at 37°C for 30 min. **Ligation –** Samples were transferred into 15ml falcons and incubated with 4860 µl sterile water, 700 µl 10× ligation buffer and 750 µl 10% Triton X-100 for 1h at 37°C (shaking). 50U ligase were added and incubated overnight at 16°C. 100 µl of the sample were taken as the “ligated control”, tested as above (5 µl of 10mg/ml Proteinase K for 2h at 65°C and phenol extraction), and compared to the “digested control” on a 0.6% agarose gel.**De-crosslinking and precipitation –** De-crosslinking was performed by adding 30 µl of 10mg/ml Proteinase K for 4h at 65°C. After 45min incubation in 30 µl RNase A (10mg/ml) at 37°C, DNA was phenol extracted and ethanol precipitated and resuspended in 150 µl 10mM Tris pH 7.5. **DpnII digestion** - HindIII-ligated 3C template was digested overnight at 37°C with DpnII (50 µl 10× restriction buffer, 50U DpnII, 300µl sterile water). DpnII was inactivated at 65°C for 30min. **Ligation and precipitation –** DNA was ligated overnight at 16°C in 12ml sterile water, 1.4ml ligation buffer, and 100U ligase. Ligation products were phenol extracted and ethanol precipitated using glycogen as a carrier (20 mg/ml), and resuspended in 75 µl 10 mM Tris pH7.5. Samples were purified using Illustra GFX PCR DNA and Gel Band Purification Kit (GE Healthcare). **PCR reaction and sequencing** - Specific primers for the *Tcra* Ea enhancer were HindIII AGACAGACCCTGCGAAGCTT and DpnII TAAGACTGGACCCACAG. The Illumina-specified adapters for Illumina GAIIx sequencing were included at the 5′ end of each primer. PCR reactions were performed using the Expand Long Template PCR system (Roche) and PCR conditions were as following: 94°C for 2 min; 30 cycles of 94°C for 1min, 55°C for 1min and 68°C for 3min; followed by

a final step of 68°C for 7min. The 4C library was sequenced on an Illumina GAIIx single-read 72-cycle run. **4C-seq analysis** - the 54bp single-end reads were aligned to a library of 40bp flanking regions of HindIII restriction sites, on the mouse genome sequence (build mm9). The alignment was performed using Maq software (http://maq.sourceforge.net/) with a quality threshold of 150. We kept the distinction between the upstream and downstream flanking region of each HindIII site. We segmented the genome according to the HindIII restriction sites and removed those segments consisting of two consecutive HindIII restriction sites that did not contain a DpnII restriction site. **Domainogram analysis –**We followed the analytical steps described previously[38], using the genomic regions enclosed between two contiguous HindIII sites. We then used windows of increasing size extending up to 30 HindIII sites. We computed and analyzed scores in each window size as follows: first we scored each pair of contiguous HindIII sites (defined as $Q(x) = (\text{rank}(x)-0.5)/N$, where Q is a quantile score of HindIII sites (x) and N is the total number of these sites). The Qi values are calculated in a global manner for the whole genome, with the bait chromosome analyzed separately. We transformed the combination of scores within each window to a form that was amenable to applying Fisher's approach for combining independent tests of significance. The range of colors in the domainograms represents the intensity of these scores. See Supplementary Table S4 for details.

ChIP-seq

ChIP-seq preparation was carried out as previously described[55] and ChIP-seq analysis was performed using the Qeseq algorithm[56] (details were provided in Chaumeil et al[40]). **Cell fixation and lysis** - $1\text{-}5\times10^6$ cells were fixed in 1% formaldehyde for 10 min at RT and lysed in 15mM Tris pH 7.5, 60mM KCl, 15mM NaCl, 15mM $MgCl_2$, 1mM $CaCl_2$, 250mM Sucrose, and 0.3% NP-40 for 10min at 4°C. Nuclei were isolated by centrifugation and washed once in “digest buffer” (10mM NaCl, 10mM Tris-HCl pH 7.5, 3mM $MgCl_2$, 1mM $CaCl_2$, 0.1 mM PMSF). **Chromatin preparation** - Mononucleosomal particles were generated using Micrococcal nuclease (USB) in “digest buffer” (reaction stopped with 20mM EDTA). Nuclei were then lysed in “nucleus lysis” buffer (50 mM Tris-HCl (pH 8.0), 10 mM EDTA (pH 8.0) and 1% SDS) and sonicated (2.5 min total; Bioruptor (Diagenode)). Chromatin was pre-cleared by addition of nine volumes of “IP dilution” buffer (0.01% SDS, 1.1% Triton X-100, 1.2 mM EDTA (pH 8.0), 16.7 mM Tris-HCl pH 8.0 and 167 mM NaCl) and magnetic Dynal beads. 1% of chromatin was saved as “input”. **Chromatin immunoprecipitation** - Antibodies (H3K4me3, Active motif; H3K9ac; Abcam) and beads were incubated together for 4 hours in “IP dilution” buffer, before overnight incubation with the chromatin at 4°C, while rotating. The complexes bound on the beads were then washed in buffers with increasing salt concentration (“wash A”: 20 mM Tris-HCl pH 8, 150 mM NaCl, 2 mM EDTA, 1% w/v Triton, 0,1% w/v SDS; “wash B”: 20 mM Tris-HCl pH 8.0, 500 mM NaCl, 2 mM EDTA, 1% w/v Triton, 0.1% w/v SDS; “wash C”: 10 mM Tris-HCl pH8.0, 250 mM LiCl, 1 mM EDTA, 1% w/v Nonidet P-40, 1% w/v deoxycholic acid) and twice with TE. The bound chromatin was cleaned using Proteinase K, at 65°C overnight and DNA was phenol extracted and ethanol precipitated. **ChIP-seq libraries and sequencing** - ChIP-seq libraries were generated using standard Illumina kit protocol. Truseq adapters were added and the libraries were PCR-amplified. Size selection was performed using E-gel electrophoresis system by Invitrogen. Cluster amplification and 36-nucleotide single-end

sequencing on an Illumina Genome Analyzer II were performed following manufacturer's instructions. **ChIP-seq analysis** - Read were aligned with Bowtie 0.12.7 software to the reference mouse genome (mouse assembly NCBI mm9), using the following command line option-best-all –m1 –n2 (reads that align uniquely in the best alignment stratum, allowing up to two mismatches).See Supplementary Table S5 for details.

Western blotting

Cells were incubated in lysing buffer (0.2% sodium dodecyl sulfate, 100mM Tris-HCL) at 16,000 cells per µl for 5 min at 95°C and treated with Bensonaze nuclease (0.05U/µl) for removal of nucleic acids for 5 min at room temperature. Protein extracts were denatured and reduced in 1× Nupage ® sample LDS and 1× Nupage ® sample reducing agent (Life Technologies) for 5 min at 95°C before the equivalent of 2×10^5 cells per lane was loaded. Membranes were blocked in phosphate-buffered saline (PBS) with 5% milk and 0.1% Tween and incubated with the following primary antibodies in 5% milk and 0.1% Tween: ATM (MAT3-4G10/8; 1/4000, Abcam) and γ-Tubulin (clone GTU-88; 1/5000, Sigma), which was used as a loading control. Blots were developed with enhanced chemiluminescence (Pierce).

Supplementary Material

Refer to Web version on PubMed Central for supplementary material.

Acknowledgments

The authors thank D. Schatz, Y. Ji and G. Teng for providing the RAG1-deficient mice, and M. Nussenzweig and D. Robbiani for the 53BP1-deficient mice. We would like to thank J. Allinne, S. Hewitt, C. Proudhon, R. Raviram, P. Rocha, M. Sellars, and T. Trimarchi for their help with 4C-seq experiments and analyses; E. Nora for his help with Image J; and members of the Skok lab for thoughtful discussions and comments on the study. This work is supported by the National Institute of Health: RO1GM086852 and R56NIAIDAI099111 (J.A.S); CA-16359 (Y.K.); RO1CA133379, RO1CA105129, RO1CA149655, RO1CA173636 and RO1GM088847 (I.A.); and CA104588 (D.B.R.). J.A.S is an LLS scholar. J.C. is an Irvington Institute Fellow of the Cancer Research Institute. M.M. was supported by an NSF IGERT 0333389. P.N. is supported by the Lady Tata Memorial Trust for Leukemia. I.A. is also supported by the Leukemia & Lymphoma Society (TRP grant), the Chemotherapy Foundation, the V Foundation of Cancer Research, and the William Lawrence Blanche Hughes Foundation, and is an early Career Scientist of the Howard Hughes Medical Institute. L.D. is supported by the Institut Pasteur, the CNRS, the Fondation pour la Recherche Medicale, the Ville de Paris, and by the European Research Council (ERC starting grant agreement #310917).

References

1. Schatz DG, Ji Y. Recombination centres and the orchestration of V(D)J recombination. Nat Rev Immunol. 2011; 11:251–263. [PubMed: 21394103]
2. Helmink BA, Sleckman BP. The response to and repair of RAG-mediated DNA double-strand breaks. Annu Rev Immunol. 2012; 30:175–202. [PubMed: 22224778]
3. Difilippantonio MJ, McMahan CJ, Eastman QM, Spanopoulou E, Schatz DG. RAG1 mediates signal sequence recognition and recruitment of RAG2 in V(D)J recombination. Cell. 1996; 87:253–262. [PubMed: 8861909]
4. Kim DR, Dai Y, Mundy CL, Yang W, Oettinger MA. Mutations of acidic residues in RAG1 define the active site of the V(D)J recombinase. Genes Dev. 1999; 13:3070–3080. [PubMed: 10601033]
5. Landree MA, Wibbenmeyer JA, Roth DB. Mutational analysis of RAG1 and RAG2 identifies three catalytic amino acids in RAG1 critical for both cleavage steps of V(D)J recombination. Genes Dev. 1999; 13:3059–3069. [PubMed: 10601032]

6. Oettinger MA, Schatz DG, Gorka C, Baltimore D. RAG-1 and RAG-2, adjacent genes that synergistically activate V(D)J recombination. Science. 1990; 248:1517–1523. [PubMed: 2360047]
7. Shinkai Y, et al. RAG-2-deficient mice lack mature lymphocytes owing to inability to initiate V(D)J rearrangement. Cell. 1992; 68:855–867. [PubMed: 1547487]
8. Liu Y, Subrahmanyam R, Chakraborty T, Sen R, Desiderio S. A plant homeodomain in RAG-2 that binds Hypermethylated lysine 4 of histone H3 is necessary for efficient antigen-receptor-gene rearrangement. Immunity. 2007; 27:561–571. [PubMed: 17936034]
9. Matthews AG, et al. RAG2 PHD finger couples histone H3 lysine 4 trimethylation with V(D)J recombination. Nature. 2007; 450:1106–1110. [PubMed: 18033247]
10. Lee GS, Neiditch MB, Salus SS, Roth DB. RAG proteins shepherd double-strand breaks to a specific pathway, suppressing error-prone repair, but RAG nicking initiates homologous recombination. Cell. 2004; 117:171–184. [PubMed: 15084256]
11. Puebla-Osorio N, Zhu C. DNA damage and repair during lymphoid development: antigen receptor diversity, genomic integrity and lymphomagenesis. Immunol Res. 2008; 41:103–122. [PubMed: 18214391]
12. Krangel MS. Mechanics of T cell receptor gene rearrangement. Curr Opin Immunol. 2009; 21:133–139. [PubMed: 19362456]
13. Ciofani M, Zuniga-Pflucker JC. Determining gammadelta versus alphass T cell development. Nat Rev Immunol. 2010; 10:657–663. [PubMed: 20725107]
14. Livak F, Tourigny M, Schatz DG, Petrie HT. Characterization of TCR gene rearrangements during adult murine T cell development. J Immunol. 1999; 162:2575–2580. [PubMed: 10072498]
15. Kurosawa Y, et al. Identification of D segments of immunoglobulin heavy-chain genes and their rearrangement in T lymphocytes. Nature. 1981; 290:565–570. [PubMed: 6783962]
16. Zha S, et al. ATM-deficient thymic lymphoma is associated with aberrant tcrd rearrangement and gene amplification. J Exp Med. 2010; 207:1369–1380. [PubMed: 20566716]
17. Deriano L, et al. The RAG2 C terminus suppresses genomic instability and lymphomagenesis. Nature. 2011; 471:119–123. [PubMed: 21368836]
18. Liang HE, et al. The “dispensable” portion of RAG2 is necessary for efficient V-to-DJ rearrangement during B and T cell development. Immunity. 2002; 17:639–651. [PubMed: 12433370]
19. Jones JM, Simkus C. The roles of the RAG1 and RAG2 “non-core” regions in V(D)J recombination and lymphocyte development. Arch Immunol Ther Exp (Warsz). 2009; 57:105–116. [PubMed: 19333736]
20. Steen SB, Han JO, Mundy C, Oettinger MA, Roth DB. Roles of the “dispensable” portions of RAG-1 and RAG-2 in V(D)J recombination. Molecular and cellular biology. 1999; 19:3010–3017. [PubMed: 10082568]
21. Qiu JX, Kale SB, Yarnell Schultz H, Roth DB. Separation-of-function mutants reveal critical roles for RAG2 in both the cleavage and joining steps of V(D)J recombination. Molecular cell. 2001; 7:77–87. [PubMed: 11172713]
22. Yarnell Schultz H, Landree MA, Qiu JX, Kale SB, Roth DB. Joining-deficient RAG1 mutants block V(D)J recombination in vivo and hairpin opening in vitro. Molecular cell. 2001; 7:65–75. [PubMed: 11172712]
23. Talukder SR, Dudley DD, Alt FW, Takahama Y, Akamatsu Y. Increased frequency of aberrant V(D)J recombination products in core RAG-expressing mice. Nucleic acids research. 2004; 32:4539–4549. [PubMed: 15328366]
24. Corneo B, et al. Rag mutations reveal robust alternative end joining. Nature. 2007; 449:483–486. [PubMed: 17898768]
25. Curry JD, Schlissel MS. RAG2's non-core domain contributes to the ordered regulation of V(D)J recombination. Nucleic acids research. 2008; 36:5750–5762. [PubMed: 18776220]
26. Bredemeyer AL, et al. ATM stabilizes DNA double-strand-break complexes during V(D)J recombination. Nature. 2006; 442:466–470. [PubMed: 16799570]
27. Rogakou EP, Pilch DR, Orr AH, Ivanova VS, Bonner WM. DNA double-stranded breaks induce histone H2AX phosphorylation on serine 139. J Biol Chem. 1998; 273:5858–5868. [PubMed: 9488723]

28. Chen HT, et al. Response to RAG-mediated VDJ cleavage by NBS1 and gamma-H2AX. Science. 2000; 290:1962–1965. [PubMed: 11110662]
29. Difilippantonio S, et al. 53BP1 facilitates long-range DNA end-joining during V(D)J recombination. Nature. 2008; 456:529–533. [PubMed: 18931658]
30. Callen E, et al. ATM prevents the persistence and propagation of chromosome breaks in lymphocytes. Cell. 2007; 130:63–75. [PubMed: 17599403]
31. Callen E, Nussenzweig MC, Nussenzweig A. Breaking down cell cycle checkpoints and DNA repair during antigen receptor gene assembly. Oncogene. 2007; 26:7759–7764. [PubMed: 18066088]
32. Meaburn KJ, Misteli T, Soutoglou E. Spatial genome organization in the formation of chromosomal translocations. Semin Cancer Biol. 2007; 17:80–90. [PubMed: 17137790]
33. Osborne CS, et al. Myc dynamically and preferentially relocates to a transcription factory occupied by Igh. PLoS Biol. 2007; 5:e192. [PubMed: 17622196]
34. Misteli T, Soutoglou E. The emerging role of nuclear architecture in DNA repair and genome maintenance. Nat Rev Mol Cell Biol. 2009; 10:243–254. [PubMed: 19277046]
35. Rocha PP, et al. Close Proximity to Igh Is a Contributing Factor to AID-Mediated Translocations. Molecular cell. 2012; 47:873–885. [PubMed: 22864115]
36. Zhang Y, et al. Spatial organization of the mouse genome and its role in recurrent chromosomal translocations. Cell. 2012; 148:908–921. [PubMed: 22341456]
37. Hakim O, et al. DNA damage defines sites of recurrent chromosomal translocations in B lymphocytes. Nature. 2012; 484:69–74. [PubMed: 22314321]
38. Bantignies F, et al. Polycomb-dependent regulatory contacts between distant Hox loci in Drosophila. Cell. 2011; 144:214–226. [PubMed: 21241892]
39. Ji Y, et al. The in vivo pattern of binding of RAG1 and RAG2 to antigen receptor loci. Cell. 2010; 141:419–431. [PubMed: 20398922]
40. Chaumeil J, et al. Higher-order looping and nuclear organization of Tcra facilitate targeted rag cleavage and regulated rearrangement in recombination centers. Cell reports. 2013; 3:359–370. [PubMed: 23416051]
41. Schoenfelder S, et al. Preferential associations between co-regulated genes reveal a transcriptional interactome in erythroid cells. Nature genetics. 2010; 42:53–61. [PubMed: 20010836]
42. Lin YC, et al. Global changes in the nuclear positioning of genes and intra- and interdomain genomic interactions that orchestrate B cell fate. Nature immunology. 2012; 13:1196–1204. [PubMed: 23064439]
43. Heard E, Bickmore W. The ins and outs of gene regulation and chromosome territory organisation. Curr Opin Cell Biol. 2007; 19:311–316. [PubMed: 17467967]
44. Fraser P, Bickmore W. Nuclear organization of the genome and the potential for gene regulation. Nature. 2007; 447:413–417. [PubMed: 17522674]
45. Splinter E, et al. The inactive × chromosome adopts a unique three-dimensional conformation that is dependent on Xist RNA. Genes Dev. 2011; 25:1371–1383. [PubMed: 21690198]
46. Kalhor R, Tjong H, Jayathilaka N, Alber F, Chen L. Genome architectures revealed by tethered chromosome conformation capture and population-based modeling. Nat Biotechnol. 2012; 30:90–98. [PubMed: 22198700]
47. Liyanage M, et al. Abnormal rearrangement within the alpha/delta T-cell receptor locus in lymphomas from Atm-deficient mice. Blood. 2000; 96:1940–1946. [PubMed: 10961898]
48. Callen E, et al. Chimeric IgH-TCRalpha/delta translocations in T lymphocytes mediated by RAG. Cell Cycle. 2009; 8:2408–2412. [PubMed: 19556863]
49. Cheutin T, Cavalli G. Progressive polycomb assembly on H3K27me3 compartments generates polycomb bodies with developmentally regulated motion. PLoS genetics. 2012; 8:e1002465. [PubMed: 22275876]
50. Hewitt SL, et al. RAG-1 and ATM coordinate monoallelic recombination and nuclear positioning of immunoglobulin loci. Nature immunology. 2009; 10:655–664. [PubMed: 19448632]

51. Johnson K, et al. IL-7 functionally segregates the pro-B cell stage by regulating transcription of recombination mediators across cell cycle. J Immunol. 2012; 188:6084–6092. [PubMed: 22581861]

52. Ward IM, Minn K, van Deursen J, Chen J. p53 Binding protein 53BP1 is required for DNA damage responses and tumor suppression in mice. Molecular and cellular biology. 2003; 23:2556–2563. [PubMed: 12640136]

53. Chaumeil J, Micsinai M, Skok JA. Combined immunofluorescence and DNA FISH on 3D-preserved interphase nuclei to study changes in 3D nuclear organization. Journal of visualized experiments : JoVE. 2013:e50087. [PubMed: 23407477]

54. Simonis M, et al. Nuclear organization of active and inactive chromatin domains uncovered by chromosome conformation capture-on-chip (4C). Nature genetics. 2006; 38:1348–1354. [PubMed: 17033623]

55. Ntziachristos P, et al. Genetic inactivation of the polycomb repressive complex 2 in T cell acute lymphoblastic leukemia. Nature medicine. 2012; 18:298–301.

56. Asp P, et al. Genome-wide remodeling of the epigenetic landscape during myogenic differentiation. Proceedings of the National Academy of Sciences of the United States of America. 2011; 108:E149–158. [PubMed: 21551099]

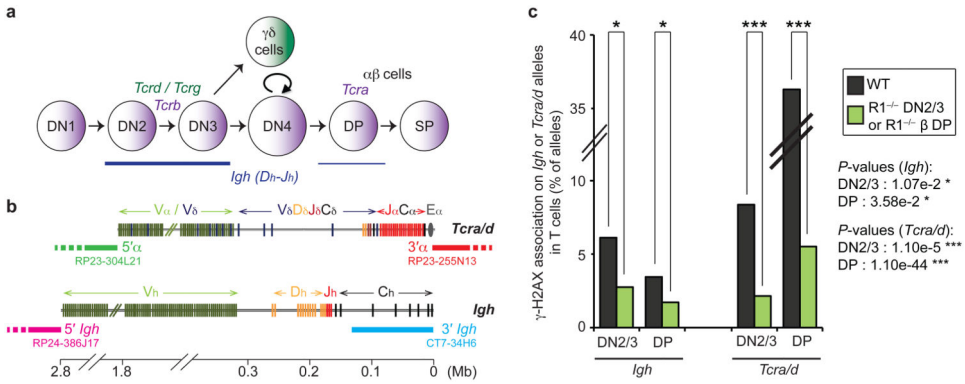

Fig. 1.

Igh* and *Tcra/d* rearrangement overlaps in DN2/3 and DP T cells**. (**a**) Scheme of T cell development with stages of recombination of the 4 *Tcr* loci. (**b**) Scheme representing the *Tcra/d* and *Igh* loci with probes for 3D-DNA FISH shown below. (**c**) Frequency of γ-H2AX association on *Igh* or *Tcra/d* alleles in WT DN2/3 and DP cells. *P*-values were calculated using a two-tail Fisher exact test (-ns- no significance ($P \geq 5.00e-2$), -*- significant ($5.00e-2 > P \geq 1.00e-2$), -**- very significant ($1.00e-2 > P \geq 1.00e-3$), -- highly significant ($P < 1.00e-3$)). Experiments were repeated at least two times and data are displayed as a combination of two independent experimental sets (n > 500 for each stage/genotype; See Supplementary Table S1 for details and individual data sets).

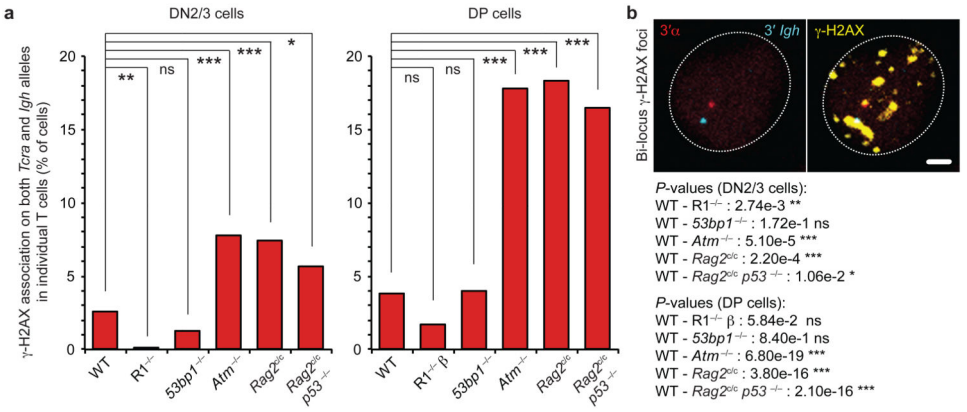

Fig. 2. The RAG2 C-terminus and ATM regulate mono-locus cleavage

(**a**) Frequency of γ-H2AX association on both *Tcra/d* and *Igh* loci in individual WT, *Rag1*$^{-/-}$ (R1$^{-/-}$ or R1$^{-/-}$ β (See Methods section for details)), *53bp1*$^{-/-}$, *Atm*$^{-/-}$, *Rag2*$^{c/c}$ and *Rag2*$^{c/c}$ *p53*$^{-/-}$ DN2/3 and DP cells. (**b**) Confocal sections showing a representative example of γ-H2AX association (in yellow) on both *Tcra/d* and *Igh* loci (3′α in red, 3′*Igh* in blue). Scale bar = 1 μm. *P*-values were calculated using a two-tail Fisher exact test (-ns- no significance ($P \geq$ 5.00e-2), -*- significant (5.00e-2 > $P \geq$ 1.00e-2), -**- very significant (1.00e-2 > $P \geq$ 1.00e-3), -***- highly significant ($P <$ 1.00e-3)). Experiments were repeated at least two times and data are displayed as a combination of two independent experimental sets (n > 200 for each stage/genotype; See Supplementary Tables S2, S3 for details and individual data sets).

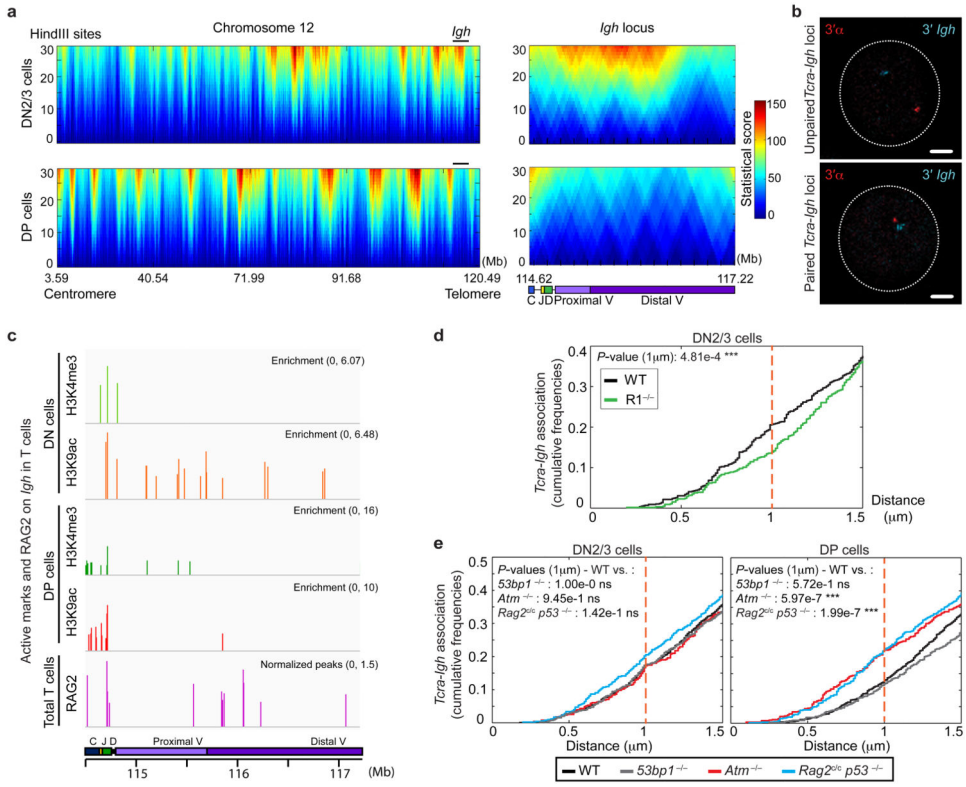

Fig. 3. The RAG2 C-terminus and ATM regulate *Tcra-Igh* association

(**a**) Domainograms showing a heatmap of *Tcra/d* interactions across the entire chromosome 12 (left) and the *Igh* locus (right) using a window size of 30 HindIII sites in DN2/3 (top) and DP (bottom) cells. See also Supplementary Fig. S2 and Table S4. (**b**) Confocal sections showing representative examples of unpaired (top) and paired (bottom) loci. 3′α in red, 3′*Igh* in blue. Scale bars = 1 μm. (**c**) Alignment of ChIP-seq data at the *Igh* locus showing levels of enrichment of H3K4me3 (green), H3K9ac (red) and RAG2 binding (purple)[39] in DN and DP cells. See also Supplementary Table S5. (**d,e**) Cumulative frequency curves of *Tcra-Igh* inter-locus distances in: WT and $R1^{-/-}$ DN2/3 cells (**d**), WT, $53bp1^{-/-}$, $Atm^{-/-}$ and $Rag2^{c/c}$ $p53^{-/-}$ DN2/3 (**e**, left) and DP (**e**, right) cells (cut-off at 1.5 μm). A left shift indicates closer association. *P*-values were calculated using a two-tail Fisher exact test (-ns- no significance ($P \geq 5.00e\text{-}2$), -*- significant ($5.00e\text{-}2 > P \geq 1.00e\text{-}2$), -**- very significant ($1.00e\text{-}2 > P \geq 1.00e\text{-}3$), -***- highly significant ($P < 1.00e\text{-}3$)). Experiments were repeated at least two times and data are displayed as a combination of two independent experimental sets (n > 200 for each stage/genotype).

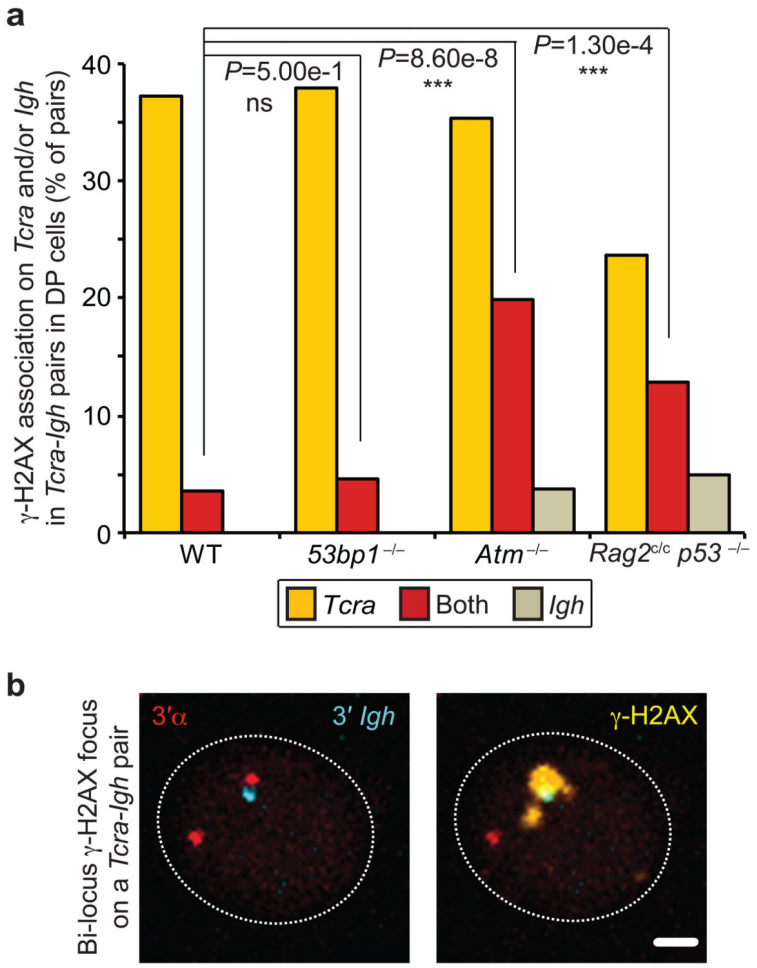

Fig. 4. RAG2 C-terminus and ATM control cleavage on *Tcra-Igh* pairs

(**a**) Frequency of γ-H2AX association on *Tcra* and/or *Igh* in *Tcra-Igh* pairs in WT, *53bp1*$^{-/-}$, *Atm*$^{-/-}$and *Rag2*$^{c/c}$ *p53*$^{-/-}$ DP cells. (**b**) Confocal sections showing a representative example of *Tcra-Igh* pair with a γ-H2AX focus on both loci. 3′α in red, 3′*Igh* in blue and γ-H2AX in yellow. Scale bar = 1 μm. *P*-values were calculated using a two-tail Fisher exact test (-ns- no significance ($P \geq$ 5.00e-2), -*- significant (5.00e-2 > $P \geq$ 1.00e-2), -**- very significant (1.00e-2 > $P \geq$ 1.00e-3), -***- highly significant ($P <$ 1.00e-3)). Experiments were repeated at least two times and data are displayed as a combination of two independent experimental sets (n > 80 for each genotype; See Supplementary Table S6 for details and individual data sets).

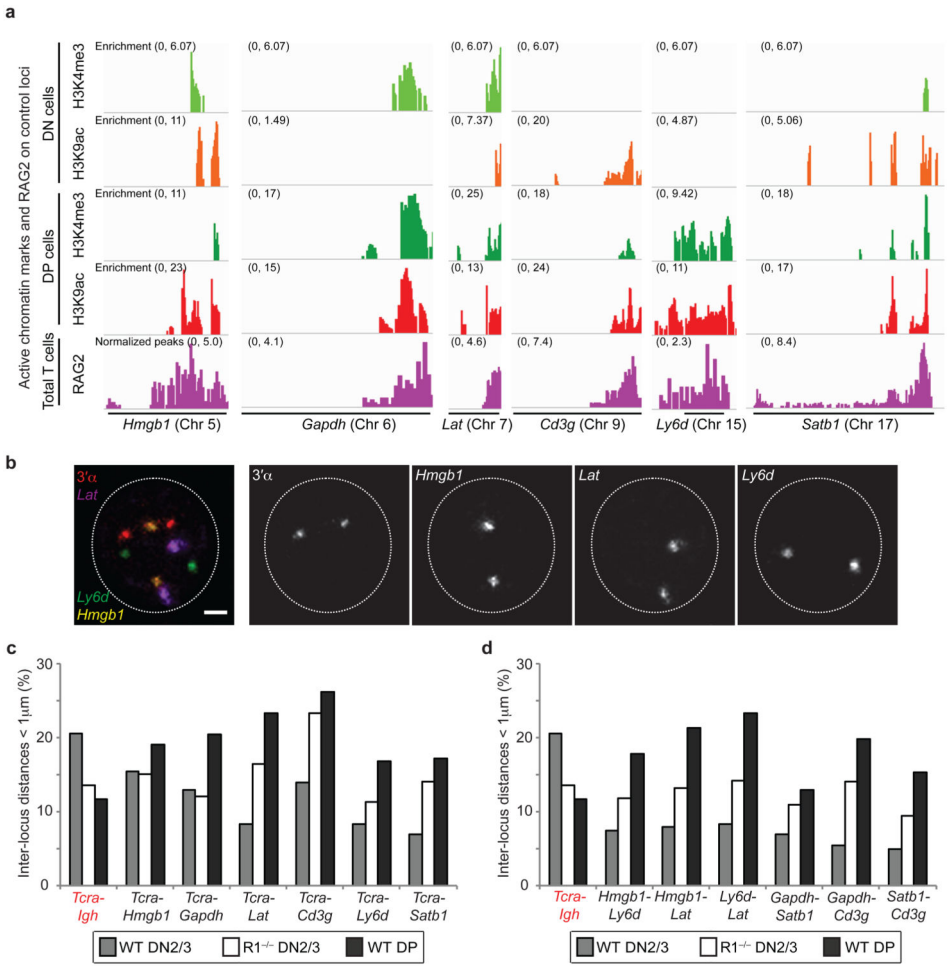

Fig. 5. RAG-mediated pairing is not a general phenomenon

(**a**) Alignment of ChIP-seq data at the *Hmgb1*, *Gapdh*, *Lat*, *Cd3g*, *Ly6d* and *Satb1* loci showing levels of enrichment of H3K4me3 (green), H3K9ac (red) and RAG2 binding (purple)[39] in DN and DP cells. (**b**) Confocal sections showing 3D DNA FISH for *Tcra* and three control loci (3′α in red, *Hmgb1* in yellow, *Lat* in purple and *Ly6d* in green. Scale bar = 1 µm. (**c,d**) Graphs showing the frequency of heterologous pairing (inter-locus distance < 1µm) between *Tcra* and the control loci (**c**), or between the loci (**d**). Experiments were performed at least one time and data are displayed as a combination of independent experimental sets when applicable (n > 200 for each stage/genotype; See Supplementary Table S7 for details).

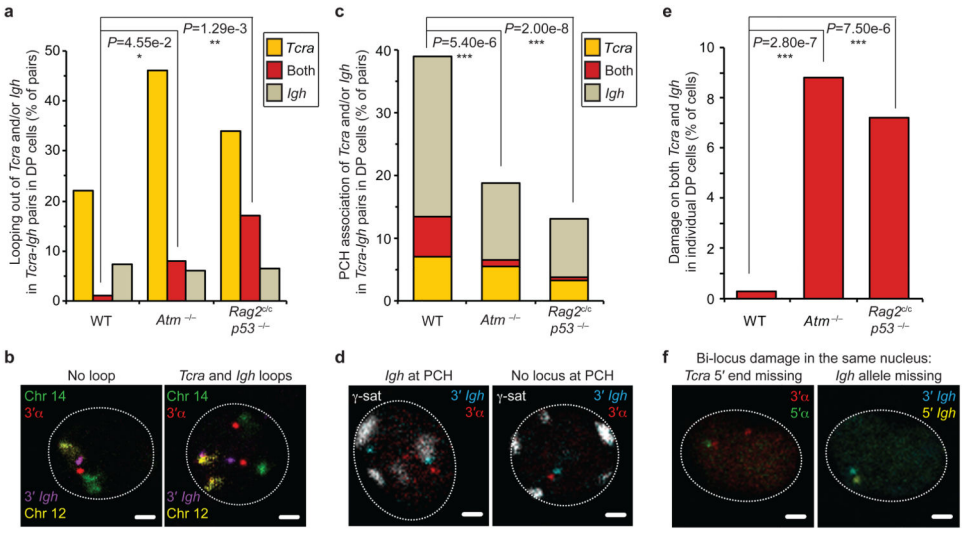

Fig. 6. Regulation of RAG cleavage is linked to genome stability

(**a**) Frequency of higher-order looping out of the 3′ ends of *Tcra* and/or *Igh* in *Tcra-Igh* pairs in WT, *Atm*$^{-/-}$and Rag2$^{c/c}$ *p53*$^{-/-}$ DP cells. (**b**) Confocal sections showing examples of *Tcra-Igh* pairs with no loop or looping of both *Tcra* and *Igh*. 3′α in red, 3′*Igh* in purple, chromosome 14 in green and 12 in yellow. Scale bars = 1 μm. (**c**) Frequency of PCH association of *Tcra* and/or *Igh* in *Tcra-Igh* pairs in WT, *Atm*$^{-/-}$and *Rag2*$^{c/c}$ *p53*$^{-/-}$ DP cells. (**d**) Confocal sections showing representative examples of *Tcra-Igh* pairs with *Igh* located at PCH or no locus at PCH. 3′α in red, 3′*Igh* in blue and γ-satellite (PCH) in white. Scale bars = 1 μm. (**e**) Frequency of cells with bi-locus damage on both *Tcra/d* and *Igh* alleles in individual WT, *Atm*$^{-/-}$and *Rag2*$^{c/c}$ *p53*$^{-/-}$ DP cells. (**f**) Confocal sections showing a representative example of bi-locus damage on both *Tcra* and *Igh* alleles in the same nucleus. One *Tcra* 5′ end and one *Igh* allele are missing. 3′α in red, 5′α in green, 3′*Igh* in blue and 5′*Igh* in yellow. Scale bars = 1 μm. *P*-values were calculated using a two-tail Fisher exact test (-ns- no significance ($P \geq$ 5.00e-2), -*- significant (5.00e-2 > $P \geq$ 1.00e-2), -**- very significant (1.00e-2 > $P \geq$ 1.00e-3), -***- highly significant ($P <$ 1.00e-3)). Experiments were repeated at least two times and data are displayed as a combination of two independent experimental sets (n > 50 for each genotype; See Supplementary Tables S8-S10 for details).